Supporting information file for

Spinel-structure catalyst catalyzing CO_2 hydrogenation to full spectrum alkenes with an ultra-high yield

Lisheng Guo [1], Jie Li [2], Yu Cui [1], Rungtiwa Kosol [1], Yan Zeng [1], Guangbo Liu [3], Jinhu Wu [3], Tiansheng Zhao [4], Guohui Yang [1], Lishu Shao [5], Peng Zhan [5], Jienan Chen [5], Noritatsu Tsubaki [1]**

[1] *Department of Applied Chemistry, School of Engineering, University of Toyama, Gofuku 3190, Toyama 930-8555, Japan*

[2] *School of Chemistry and Chemical Engineering, Yangzhou University, Yangzhou 225002, China*

[3] *Qingdao Institute of Bioenergy and Bioprocess, Chinese Academy of Sciences, Qingdao, 266101, China*

[4] *State Key Laboratory Cultivation Base of Natural Gas Conversion, Ningxia University, Yinchuan, 750021, China*

[5] *Ministry of Forestry Bioethanol Research Center, Central South University of Forestry and Technology, Changsha, 410004, China*

Corresponding authors: chenjnx@163.com; tsubaki@eng.u-toyama.ac.jp

Total number of Pages: 20 (S1-S20)

Total number of Figures: 12 (Figure S1-Figure S12)

Total number of Tables: 5 (Table S1-Table S5)

Catalyst preparation

All spinel-like catalysts were fabricated through solvent-thermal synthesis. In brief, iron (III) nitrate nonahydrate of 2.02 g and zinc nitrate hexahydrate of 0.74 g (Zn/Fe=1:2 molar ratio) were dissolved in distilled water (40 mL), and NaOH (0.1 mol) was added to the mixtures to ensure that it was basic. The solution was transferred to a 100 mL Teflon tube being set in a stainless autoclave, which was then placed in oven for 8 h at 180 ^{0}C for the synthesis reaction. After the sample cooled to ambient temperature, it was washed with distilled water (0.5L) to control the amount of residual Na, denoted as Na-$ZnFe_2O_4$. If KOH replaces NaOH, another catalyst can be obtained by the same procedures, labeled as K-$ZnFe_2O_4$. When NaOH or KOH was replaced by $NH_3{\cdot}H_2O$, the corresponding catalysts was marked as $ZnFe_2O_4$ to compare with the catalytic performance derived from promoter modified one. Different from K-$ZnFe_2O_4$ preparation process, iron (III) nitrate nonahydrate of 1.616 g, cobaltous nitrate hexahydrate of 0.291 g, and zinc nitrate hexahydrate of 0.74 g (Zn/(Fe+Co) = 1:2 molar ratio, Fe/Co = 4:1 molar ratio) were dissolved in distilled water (40 mL), and KOH (0.1 mol) was used. Following the same procedures, the resulting catalyst was labeled as K-$Zn(FeCo)_2O_4$. Besides, the reference catalyst (Fe_2O_3) was also prepared through solvent-thermal synthesis method, in which $NH_3{\cdot}H_2O$ was adopted to eliminate the effects of promoter. To clarity the beneficial $ZnFe_2O_4$ structure, ZnO+Fe_2O_3 catalyst was also fabricated. Briefly, same mole of ZnO and Fe_2O_3 was physically mixed to form a catalyst with the same composition as the spinel structure ($ZnFe_2O_4$), marked as ZnO+Fe_2O_3 catalyst.

Catalyst characterization

Powder X-ray diffraction (XRD) of the catalysts was recorded on a Rigaku RINT 2400 X-ray diffractometer using Cu Kα irradiation at 40 kV and 40 mA. Patterns were collected in the 2θ range of 5−90° with a scanning step length of 0.02 deg/s. The X-ray photoelectron spectroscopy (XPS) analysis was conducted on Thermo Fisher Scientific ESCALAB 250Xi multifunctional X-ray photoelectron spectroscope with pretreatment chamber. The temperature-programmed desorption (CO_2-TPD) and temperature-programmed reduction (H_2-TPR) of the as-prepared catalysts were characterized over a BELCAT-II-T-SP Characterization System. Scanning electron microscopy (SEM) images and element mapping were carried out on a JEOL JSM-6360LV microscope equipped with energy dispersive spectrometer (EDS). The accelerating voltage was 10 kV. High-resolution transmission electron microscopy (HRTEM) for spent catalysts was obtained using a TOPCON EM-002B at 120 kV. N_2 physisorption was performed on a Micromeritics analyzer. Before sample analysis, the catalysts (50 mg) were vacuum-dried at 200 °C for 6 h. Shimadzu DTG-60 for thermal gravity analysis (TGA) was used to measure weight changes of spent catalysts when heated under a O_2/N_2 flow (21 vol %/79 vol %, 30 ml min^{-1}) at a constant beating rate of 5 °C min^{-1}.

Catalyst reaction

CO_2 hydrogenation processes over as-prepared catalysts were measured in a fixed-bed stainless steel reactor (6.0 mm inner diameter). First, the as-prepared catalysts (0.5 g) were *in situ* reduced at 400 °C for 10 h in a pure H_2 flow (40 mL min^{-1}). Subsequently, the temperature was dropped to certain reaction temperature. After that, the reactant gas of $CO_2/H_2/Ar$ (27.1 vol %/67.6 vol %/5.3 vol %) was fed into the reactor, and the pressure increased to 2.0 MPa. N-octane in ice-trap as solvent could catch and collect the liquid hydrocarbons from the effluents. After reaction finished, the obtained liquid hydrocarbons were analyzed by an off-line gas chromatograph using a flame ionization detector. CO_2 conversion, CO selectivity, and hydrocarbons selectivity were calculated according to equation 1, 2, and 3, respectively.

$$CO_{2\ conversion\ (\%)} = \frac{CO_{2\ in} - CO_{2\ out}}{CO_{2\ in}} \times 100\% \quad (1)$$

$CO_{2\ in}$: mole fraction of CO_2 in the inlet, $CO_{2\ out}$: mole fraction of CO_2 in the outlet.

$$CO_{\ selectivity\ (\%)} = \frac{CO_{\ out}}{CO_{2\ in} - CO_{2\ out}} \times 100\% \quad (2)$$

$CO_{\ out}$: mole fraction of CO in the outlet.

$$C_{i\ hydrocarbon\ selectivity\ (C-mol\ \%)} = \frac{\text{Mole of } C_i \text{ hydrocarbons} \times i}{\sum_{i=1}^{n} \text{Mole of } C_i \text{ hydrocarbons} \times i} \times 100\% \quad (3)$$

Table S1. Catalytic performance of CO_2 hydrogenation over different catalysts. [a]

Catalysts	CO_2 Conv. (%)	CO Sel. (%)	Selectivity (mol-%)			Alkenes Sel. (%) [b]	O/(O+P) [c] (%)
			CH_4	C_{2-4}	C_{5+}		
Fe_2O_3	32.8	6.3	42.7	48.5	8.8	7.4	12.9
$ZnFe_2O_4$	41.3	8.1	33.3	52.0	14.7	25.4	38.1
Na-$ZnFe_2O_4$	46.7	9.2	15.0	51.0	34.0	68.0	80.0
K-$ZnFe_2O_4$	47.1	8.7	14.8	39.1	46.1	68.9	83.6
K-$Zn(FeCo)_2O_4$	60.4	4.5	28.0	51.3	20.7	57.5	80.0

[a]Reaction conditions: 320 °C, 2.0 MPa, H_2/CO_2=2.5, W/F=10 g h^{-1} mol^{-1}; [b]Alkenes Sel. (%) represents alkene selectivity in whole hydrocarbon; [c]O/(O+P) stands for the molar ratio of $C_{2+}^{=}/(C_{2+} + C_{2+}^{=})$.

Table S2. Catalytic performance of CO_2 hydrogenation over different catalysts. [a]

Catalysts	CO_2 Conv. (%)	CO Sel. (%)	Selectivity (mol-%)			Alkenes Sel. (%) [b]	O/(O+P) [c] (%)
			CH_4	C_{2-4}	C_{5+}		
$ZnFe_2O_4$	41.3	8.1	33.3	52.0	14.7	25.4	38.1
$ZnO+Fe_2O_3$	37.9	13.4	46.3	46.8	6.9	2.0	3.7

[a]Reaction conditions: 320 ^oC, 2.0 MPa, H_2/CO_2=2.5, W/F=10 g h^{-1} mol^{-1}; [b]Alkenes Sel. (%) represents alkene selectivity in whole hydrocarbon; [c]O/(O+P) stands for the molar ratio of $C_{2+}^{=}/(C_{2+} + C_{2+}^{=})$.

Table S3. Surface area of different iron-based catalysts.

Samples	Surface area (m^2/g)
Fe_2O_3	15.4
$ZnFe_2O_4$	38.3
Na-$ZnFe_2O_4$	138.1
K-$ZnFe_2O_4$	119.3
K-$Zn(FeCo)_2O_4$	139.2

Table S4. Catalytic performance of CO_2 hydrogenation over a multi-stage reactor system.

Catalysts	Stage	W/F ($g\ h^{-1}\ mol^{-1}$)	T (°C)	P (MPa)	CO_2 Conv. (%)	CO Sel. (%)	Selectivity (mol-%)			STY ($g/kg_{cat}\ h$)	
							CH_4	C_{2-4}	C_{5+}	C_{5+}	$C_{2+}^{=}$
K-$ZnFe_2O_4$	2	2.5	320	2.0	55.9	6.4	16.5	43.8	39.7	334.9	598.6
K-$ZnFe_2O_4$	2	2.5	320	2.0	55.9	6.4	16.5	43.8	39.7	334.9	598.6
K-$ZnFe_2O_4$	2	2.0	320	2.0	50.6	9.9	17.4	43.4	39.2	353.0	619.0
K-$ZnFe_2O_4$	2	2.0	340	2.0	60.0	5.6	16.7	40.6	42.7	487.6	797.5
K-$ZnFe_2O_4$	2	2.0	360	2.0	66.1	5.8	24.4	42.7	32.9	412.1	799.1
K-$ZnFe_2O_4$	3	2.0	320	2.0	66.3	4.0	13.5	37.1	49.4	632.7	923.1
K-$ZnFe_2O_4$	3	2.0	340	2.0	76.7	2.3	13.5	33.5	53.0	787.4	1086.8

Notes: Stage 2 stands for a two-stage reactor system while stage 3 stands for a three-stage reactor system.

Table S5. Catalytic performance of CO_2 hydrogenation over different catalysts.

Catalysts	Stage	GHSV (mL h^{-1} g_{cat}^{-1})	T (°C)	P (MPa)	CO_2 Conv. (%)	CO Sel. (%)	Selectivity (mol-%)			STY (g/kg_{cat} h)	
							CH_4	C_{2-4}	C_{5+}	C_{5+}	$C_{2+}^{=}$
Wei et al.[1]	1	4000	320	3.0	34.0	14.0	8.0	18.0	74.0	145.0	180.0[a]
Gao et al.[2]	1	9000	340	3.0	19.0	48.0	1.0	27.6	71.4	106.4	147.6[b]
Gnanamani et al.[3]	1	2000	270	0.9	22.6	53.0	65.5	25.1	9.4	3.5	12.9[c]
Wei et al.[4]	1	2000	320	3.0	40.5	13.5	15.8	54.1	30.1	31.4	87.8[d]
Choi et al.[5]	1	1800	300	1.0	18.1	31.9	3.9	35.8	60.3	20.8	33.1[e]
Choi et al.[6]	1	1800	340	1.0	27.8	21.9	9.7	31.8	58.5	35.5	50.3
Gao et al.[7]	1	12000	400	1.5	13.0	84.0	2.0	98.0	0.0	0	38.0
Gao et al.[8]	1	15750	400	3.0	34.0	83.0	5.0	93.0	2.0	2.7	131.6[f]
Li et al.[9]	1	3600	380	2.0	47.0	12.0	3.0	95.0	2.0	4.4	181.9
Liu et al.[10]	1	3600	400	3.0	46.1	17.5	32.3	26.9	40.8	83.2	138.1[g]
Visconti et al.[11]	1	4100	300	0.5	45.0	12.0	18.2	81.8[h]	N.G.	N.G.	205.1[i]
Liang et al.[12]	1	2040	320	3.0	39.3	9.0	8.9	31.2	59.9	67.8	92.0
Li et al.[13]	1	3600	400	3.0	41.7	26.5	37.8	43.4	18.8	32.3	106.5[j]
Boreriboon et al.[14]	1	3600	300	1.1	23.9	31.0	33.3	16.0	50.7	44.9	59.0[k]
Kishan et al.[15]	1	1900	300	1.0	27.5	18.6	28.2	46.3	25.5	18.2	51.2[l]
Nam et al.[16]	1	1900	300	1.0	26.5	4.4	24.3	58.4	17.3	12.9	56.4[m]
Guo et al.[17]	2	9200	300	3.0	65.1	3.3	21.0	40.4	38.5	227.4	466.6[n]
Our work	3	12000	340	2.0	76.7	2.3	13.5	33.5	53.0	787.4	1086.8
Our work	3	24000	340	2.0	70.8	3.7	19.2	44.5	36.3	1000.5	1858.1

Notes: a. C_{2+} products; b. C_{2+} products; c. C_{2+} products; d. C_{2+} products; e. C_{2+} products; f. C_{2+} products; g. C_{2+} products; h. C_{2+} products; i. C_{2+} products; j. C_{2+} products; k. C_{2+} products; l. C_{2+} products; m. C_{2+} products; n. C_{2+} products.

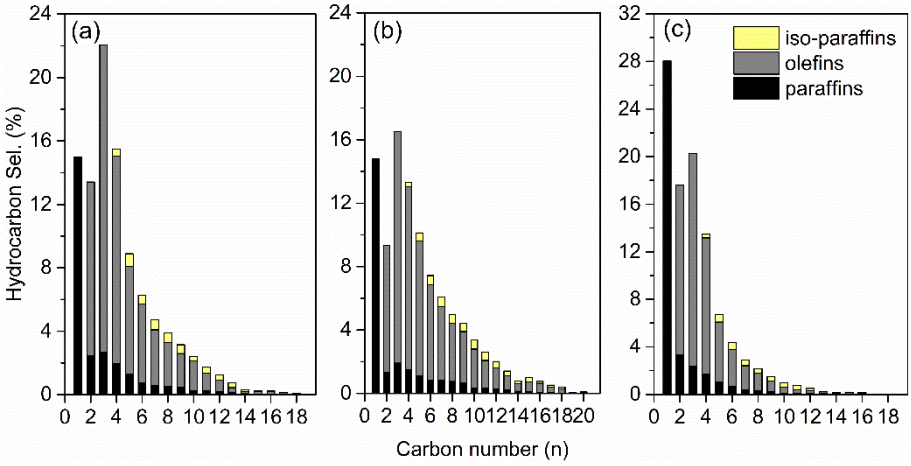

Fig. S1. Product distribution from different spent iron-based catalysts. (a, Na-$ZnFe_2O_4$; b, K-$ZnFe_2O_4$; c, K-$Zn(FeCo)_2O_4$)

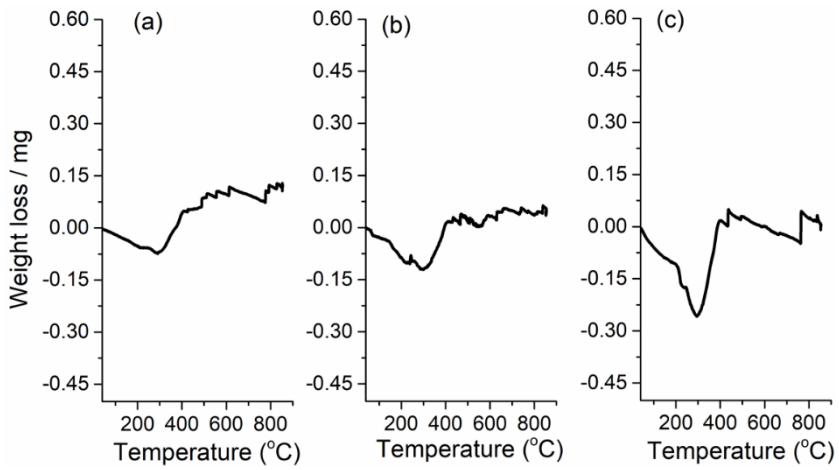

Fig. S2. Weight loss of different iron-based catalysts after 36h reaction with an N_2/O_2 = 4. (a, Na-$ZnFe_2O_4$; b, K-$ZnFe_2O_4$; c, K-$Zn(FeCo)_2O_4$, data collected from TG profiles)

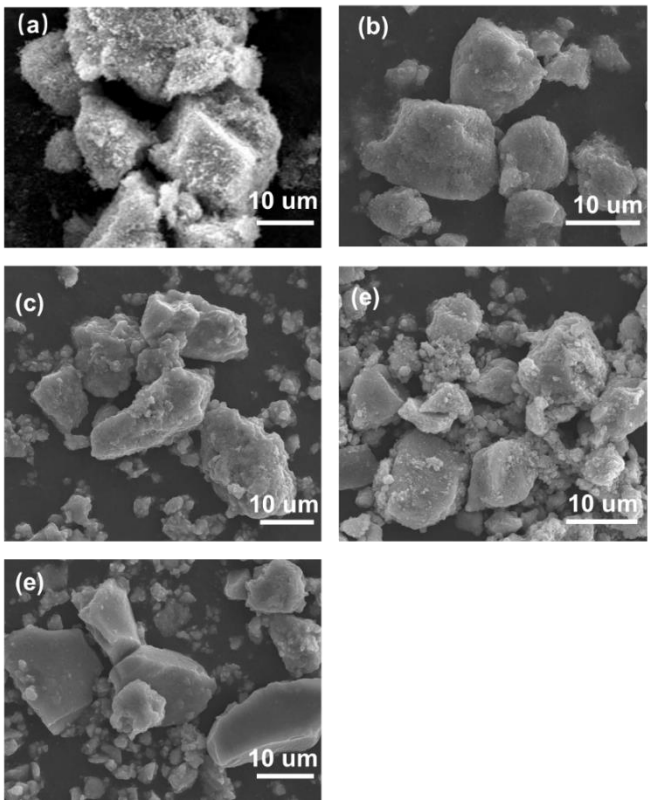

Fig. S3. Typical SEM images of different as-prepared iron-based catalysts. (a, Fe_2O_3; b, $ZnFe_2O_4$; c, Na-$ZnFe_2O_4$; d, K-$ZnFe_2O_4$; e, K-$Zn(FeCo)_2O_4$)

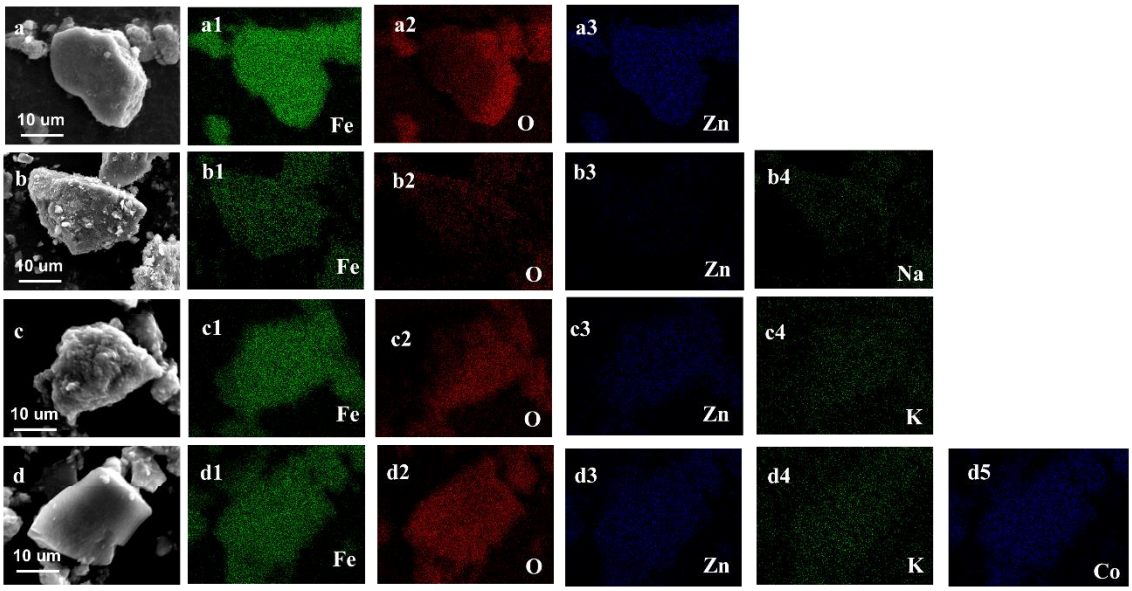

Fig. S4. Special SEM images and corresponding element composition mapping of different spinel-like catalysts. (a, $ZnFe_2O_4$; b, Na-$ZnFe_2O_4$; c, K-$ZnFe_2O_4$; d, K-$Zn(FeCo)_2O_4$)

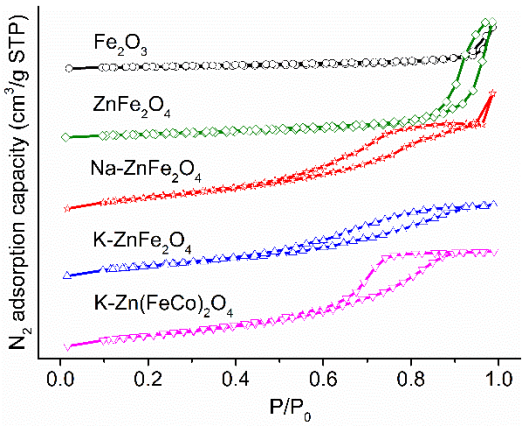

Fig. S5. N_2 adsorption-desorption isotherms of different iron-based catalysts.

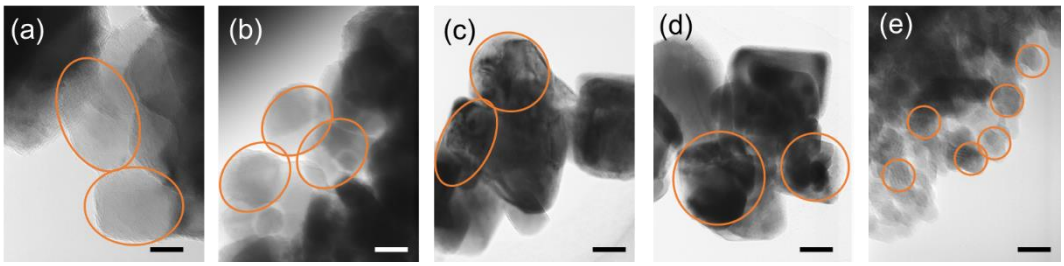

Fig. S6. Typical TEM images of different spent catalysts. (a. Fe_2O_3; b. $ZnFe_2O_4$; c. Na-$ZnFe_2O_4$; d. Na-$ZnFe_2O_4$; e. K-$Zn(FeCo)_2O_4$; besides, the stand bars in the pictures stand for 10 nm) The orange circles that marked in figures stand for the particle sizes of different spent catalysts.

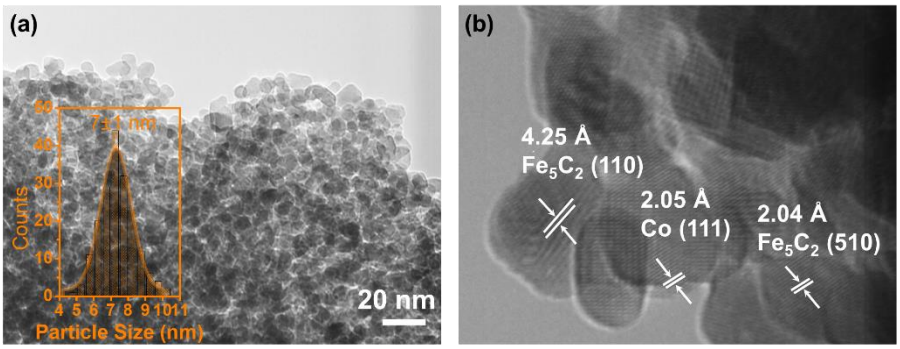

Fig. S7. Typical TEM images of spent K-Zn$(FeCo)_2O_4$.

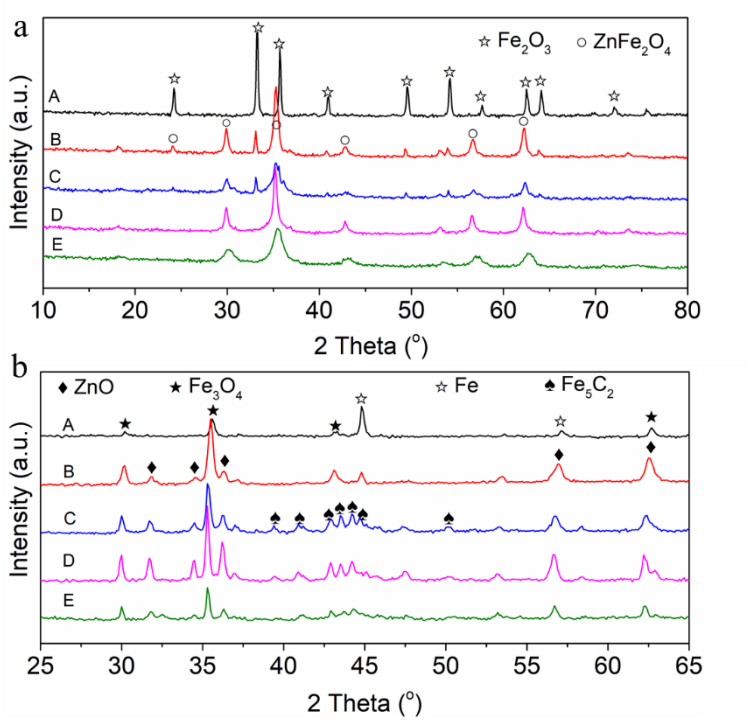

Fig. S8. XRD patterns of fresh (a) and spent (b) catalysts. (A, Fe_2O_3; B, $ZnFe_2O_4$; C, Na-$ZnFe_2O_4$; D, K-$ZnFe_2O_4$; E, K-$Zn(FeCo)_2O_4$)

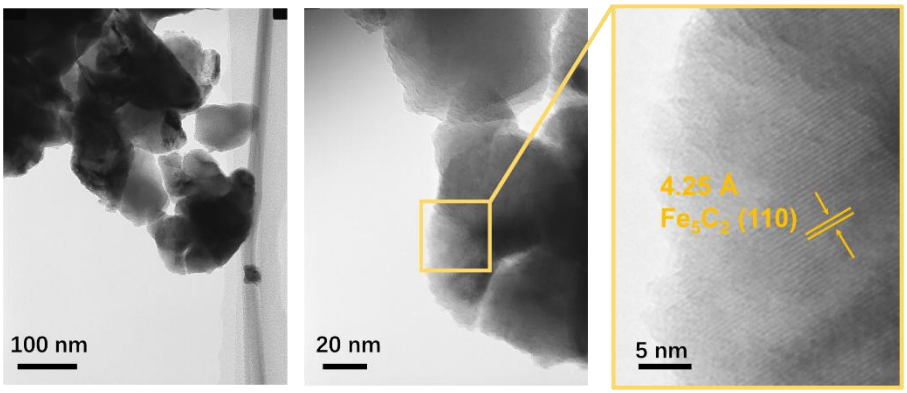

Fig. S9. HR-TEM images of spent Fe_2O_3 catalysts.

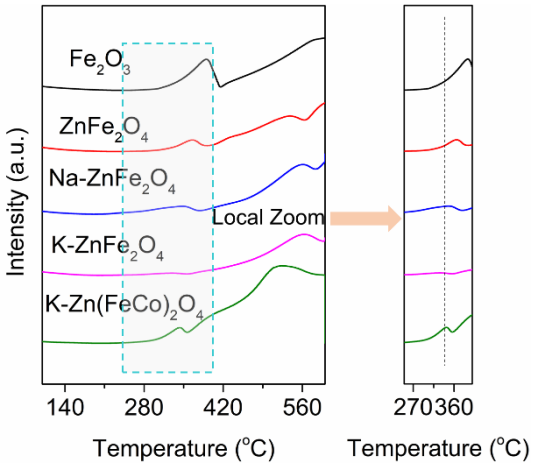

Fig. S10. H_2-TPR curves of different catalysts.

Usually, the reduction of a catalyst can be regarded as the first step of a phase composition change, followed by further generation of active sites. Hence, the H_2-TPR patterns of different catalysts are compared and shown in Fig. S10. Compared with Fe_2O_3, both $ZnFe_2O_4$ and Na–$ZnFe_2O_4$ show a slight shift to the low temperature (LT) region. However, for the K–$Zn(FeCo)_2O_4$ catalyst, the two peaks obviously shift toward the LT region, which indicates that the further doping of Co metal results in a favorable reduction behavior.

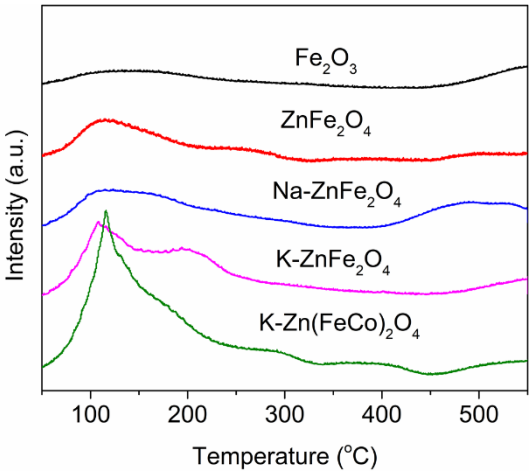

Fig. S11. CO_2-TPD curves of different catalysts.

The desorption experiment of CO_2 (CO_2–TPD) was carried out and the results are shown in Fig. S11 and S12. According to Fig. S11, it can be found that the absorption amount of CO_2, from both weak adsorption and medium-strength adsorption, is evidently enhanced with the introduction of the Zn structural promoter. With the further introduction of the electronic promoter, the adsorption strength of CO_2 is well regulated. However, when cobalt metal is introduced into the catalyst system, CO_2 adsorption capacity increases obviously (Fig. S11).

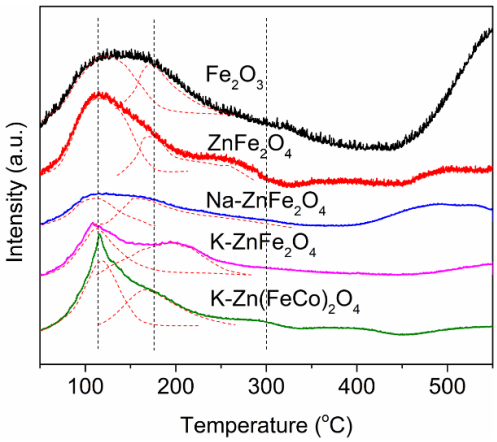

Fig. S12. CO_2-TPD curves normalized by relative surface area content of different catalysts.

To take the surface area into account, the CO_2–TPD curves normalized by relative surface area are shown in Fig. S12. Compared to the Fe_2O_3 catalyst, for the $ZnFe_2O_4$ catalyst, the content of the medium strength adsorption peak located in the range of 150 to 300 °C is improved compared with that of the weak adsorption peak (50 to 150 °C). In the presence of an electronic promoter, especially K, the adsorption peak of medium strength is strengthened obviously. However, weak CO_2 adsorption is not conducive to the activation and utilization of reactive molecules; hence, this improved adsorption can drive the improvement of activity and target alkene. Besides, the K–$Zn(FeCo)_2O_4$ catalyst also still maintains a high relative adsorption content, i.e. a strong medium strength adsorption peak.

Reference

1. J. Wei, Q. Ge, R. Yao, Z. Wen, C. Fang, L. Guo, H. Xu, J. Sun, Nat. Commun., 2017, 8, 15174-15181.
2. P. Gao, S. Li, X. Bu, S. Dang, Z. Liu, H. Wang, L. Zhong, M. Qiu, C. Yang, J. Cai, W. Wei, Y. Sun, Nat. Chem., 2017, 9, 1019-1024.
3. M.K. Gnanamani, G. Jacobs, H.H. Hamdeh, W.D. Shafer, F. Liu, S.D. Hopps, G.A. Thomas, B.H. Davis, ACS Catal., 2016, 6, 913-927.
4. J. Wei, J. Sun, Z. Wen, C. Fang, Q. Ge, H. Xu, Catal. Sci. Technol., 2016, 6, 4786-4793.
5. Y.H. Choi, Y.J. Jang, H. Park, W.Y. Kim, Y.H. Lee, S.H. Choi, J.S. Lee, Appl. Catal., B, 2017, 202, 605-610.
6. Y.H. Choi, E.C. Ra, E.H. Kim, K.Y. Kim, Y.J. Jang, K.-N. Kang, S.H. Choi, J.-H. Jang, J.S. Lee, ChemSusChem, 2017, 10, 4764 -4770.
7. J. Gao, C. Jia, B. Liu, Catal. Sci. Technol., 2017, 7, 5602-5607.
8. P. Gao, S. Dang, S. Li, X. Bu, Z. Liu, M. Qiu, C. Yang, H. Wang, L. Zhong, Y. Han, Q. Liu, W. Wei, Y. Sun, ACS Catal., 2017, 8, 571-578.
9. Z. Li, J. Wang, Y. Qu, H. Liu, C. Tang, S. Miao, Z. Feng, H. An, C. Li, ACS Catal., 2017, 7, 8544-8548.
10. J. Liu, A. Zhang, S.H. Min Liua, F. Ding, C. Song, X. Guo, J CO2 Util., 2017, 21, 100-107.
11. C.G. Visconti, M. Martinelli, L. Falbo, A. Infantes-Molina, L. Lietti, P. Forzatti, G. Iaquaniello, E. Palo, B. Picutti, F. Brignoli, Appl. Catal., B, 2017, 200, 530-542.
12. B. Liang, T. Sun, J. Ma, H. Duan, L. Li, X. Yang, Y. Zhang, X. Su, Y. Huang, T. Zhang, Catal. Sci. Technol., 2019, 9, 456-464.
13. J. Liu, A. Zhang, X. Jiang, M. Liu, Y. Sun, C. Song, X. Guo, ACS Sustainable Chem. Eng., 2018, 6, 10182-10190.
14. N. Boreriboon, X. Jiang, C. Song, P. Prasassarakich, J CO2 Util., 2018, 25, 330-337.
15. G. Kishan, M.-W. Lee, S.-S. Nam, M.-J. Choi, K.-W. Lee, Catal. Lett., 1998, 56, 215-219.
16. S.-S. Nam, S.-J. Lee, H. Kim, K.-W. Jun, M.-J. Choi, K.-W. Lee, Energy Convers. Mgmt., 1997, 38, 397-402.
17. L. Guo, Y. Cui, P. Zhang, X. Peng, Y. Yoneyama, G. Yang, N. Tsubaki, ChemistrySelect, 2018, 3, 13705-13711.